41st Aerospace Sciences Meeting and Exhibit
6-9 January 2003, Reno, Nevada

AIAA-2003-0918

ASSESSMENT OF PARTICLE SEEDER PERFORMANCE VIA DIRECT FLOWFIELD SAMPLING

Z.C. Owens*, C.P. Goyne†, R.H. Krauss‡ and J.C. McDaniel§
University of Virginia, Charlottesville, VA 22904-4248

ABSTRACT

In this experimental study, fine Alumina particles were sampled from a seeded gaseous flow and then imaged to obtain shape and size information. The seeding apparatus used in the study was employed in previous Particle Image Velocimetry (PIV) and Fuel Plume Imaging (FPI) experiments in a supersonic combustor. The present experiment provided an opportunity to assess the performance of the seeding apparatus and to draw conclusions on the effect of particle size distribution on PIV and FPI type measurements. In the experiment, helium and nitrogen were adopted as the gases to be seeded in order to safely simulate the seeded hydrogen fuel of the previous supersonic combustion experiments. In addition, the choice of two different gases allowed the influence of the gas thermodynamic properties on the particle size distribution to be investigated. Seeded particles were sampled from an underexpanded free jet using a sampling tube and were collected via filter paper. Particle shape information and size distributions were then determined from images obtained using a Scanning Electron Microscope (SEM). The experimental results revealed that particle shapes were irregular, ligamental or rounded in nature. In addition, given the use of a particle-shearing nozzle in the seeder, the average size of the collected particles was inversely proportional to the speed of sound of the seeded gas. For helium, the average seeded particle size was 0.23 μm, while for nitrogen, the average size was 0.49 μm. This compares with a manufacturer specified nominal primary particle size of 0.3 μm. The experimental results confirmed the expected behavior of the seeding apparatus. Namely, an extent of particle agglomerate breakdown was dependent on seeded gas speed of sound. It was further shown, using a combination of the particle distribution data and Mie scattering theory, that a very small proportion of large particles can still dominate a scattered light intensity signal. Lastly, it was demonstrated how particle distribution data can be used to assess the contribution of particle lag errors to the experimental uncertainty of a particle based diagnostic.

INTRODUCTION

Particle based flow diagnostics, such as Particle Image Velocimetry (PIV) and Fuel Plume Imaging (FPI), are popular techniques used by experimentalists to interrogate complex flowfields. Both methods have been used at the University of Virginia to study the mixing and combustion processes in a scramjet combustor[1,2]. Of fundamental importance to both techniques is the microscopic particle that is seeded into the flowfield. In both PIV and FPI the light scattering properties of the particles are exploited in order to collect meaningful data regarding the state of the flow. In order for the techniques to be accurate, the seeding apparatus must distribute appropriately sized particles into the flowfield. Too large a particle will not respond quickly enough to sudden changes in the flow velocity, and this poor tracking will cause erroneous data. This is particularly important for applications involving high speed flows, such as the experiments of Refs. 1 and 2. If the particle is too small, it will not scatter sufficient light to provide a signal-to-noise ratio high enough to minimize measurement uncertainties in the signal processing[3,4]. Theoretical techniques exist for predicting a size range in which particles will accurately track a given flowfield and still remain detectable. However, the need still remains for an experimental technique that will allow researchers to assess whether their particle seeders are actually delivering particles in this prescribed range.

Particle size uncertainty exists because particles tend to form agglomerates when stored, and if these agglomerates are not fully broken down by the seeder, particle diameters will not match the manufacturer's nominal specifications. Therefore, the goal of this work was to develop an experimental technique to assess seeded particle size and apply it to the particle seeder used by Refs. 1 and 2. To this end, a technique was developed to sample particles directly from a seeded flow and to then determine the particle size distribution. This was achieved by developing a sampling tube and filter paper apparatus that could capture particles from a seeded flowfield in an unbiased manner. Sampled particles were then interrogated using a Scanning Electron Microscope (SEM).

---

* Undergraduate Research Assistant, currently Graduate Research Assistant, Stanford University, Student Member AIAA
† Research Scientist, Member AIAA
‡ Research Consultant
§ Professor, Senior Member AIAA

Previous Work

The determination of particle size once particles have been seeded into a gas flow has not been the subject of extensive experimental investigation. Reference 4 was one of the first works to assess the actual particle size distribution after injection into a flowfield. This was attempted in two ways. The first involved comparing a theoretical prediction of a given particle trajectory in a known flowfield to the trajectory actually measured using laser velocimetry. After the experimental results were obtained, the size of the particle in the theoretical model could then be iteratively adjusted until the model trajectory matched the measured data. In this way, Ref. 4 could estimate the effective average size of the particle. However, this method is prone to inaccuracies because the accelerative forces and viscous resistance as modeled in the simulation are based on Stokes' law, which assumes completely spherical particles[4]. Such particles may not be spherical.

A second method of assessing size distributions involved using an optical particle size analyzer. Though this system was not described in explicit detail by Ref. 4, it is suggested that the device correlated an average light reflectance to an average particle size. Ref. 4 pointed out that light reflectance is not solely a function of particle size but also very sensitive to particle orientation. Only spherical particles will reflect light independent of orientation; however, as mentioned above, such particles may not be spherical. Thus, this method also gives only approximate distributions. As evident above, particle shape is an important parameter, and consequently the present investigation considers the shape of sampled particles, as well as size distribution.

The need for a more direct method of assessing particle size distributions surfaced again in a study described in Ref. 5. This work assessed particle sizes by analyzing SEM images of particles before they were processed by the seeder. A major recommendation of this study was the need to assess a final, seeded size distribution.

More recent efforts at assessing particle size distributions are presented in Ref. 1. Here, the method of sampling involved manually exposing a small strip of double-sided adhesive tape to a seeded flowfield. The tape surface was then scanned with an electron microscope in order to estimate the size and distribution of the particles collected. A major problem in this method of sampling was that the sampling surface was biased towards the collection of larger particles. This is because smaller particles were able to react more quickly to rapid changes in the flowfield. As a result, they were more likely to follow the flow around the adhesive surface rather than adhering to the surface. On the other hand, large particles had a higher probability of impacting the sampling surface because of their relatively poor tracking ability. While this study did estimate a minimum particle size, the overall results were approximate and inconclusive.

Objectives

The ultimate goal of the study presented herein is to reduce the uncertainty of the particle based measurement techniques as conducted in investigations such as Ref. 1 and 2. This was achieved through the accomplishment of the following primary objectives:

1. Development of an unbiased particle-sampling apparatus,
2. Determination of output particle shape and size for two different seeded gases, thus enabling an analysis of the effect of seeded gas properties on seeder performance, and,
3. Assessment of the effect of particle size distribution on experimental uncertainty caused by particle lag.

This paper begins by describing the particle sampling apparatus that was developed for the present study. Experimental and image processing methods are then discussed. Results for the study are then presented in terms of observed particle shape, particle size distributions and expected light scattering distributions. An example of the effect of size distribution on particle tracking behavior in a high speed flow is then presented before moving on to the conclusion.

EXPERIMENT

Apparatus

The experimental setup adopted in this study consisted of the nine primary components that are illustrated in Fig. 1. The first four of these components supplied a seeded, under-expanded free jet of gas at a known total pressure. These components consisted of a gas cylinder and regulator, the particle seeding apparatus, a pressure gauge and an exhaust nozzle. The five remaining components formed the particle sampling apparatus. These components consisted of a sampling probe, a motorized translation stage, a primary and secondary filter and a vacuum pump. The vacuum pump was used to maintain flow through the sampling probe and thus prevent stagnation conditions at the inlet plane of the probe. The design and operation of the major components of the experiment are discussed below.

Particle seeder

The seeding apparatus is schematically presented in Fig. 2. The seeder operated with a fluidizer, a fine pickup tube and a particle-shearing nozzle in order to achieve particle

de-agglomeration and seeding. When flow entered the seeder inlet it was immediately separated into two paths, one lead to the base of the fluidizer (Path B) and the other directly to the particle-shearing nozzle (Path A). A greater proportion of the flow followed Path A and was accelerated to Mach 3 in the particle-shearing nozzle. At some point downstream of the nozzle, the flow shocked back to subsonic flow. The remaining proportion of the flow was directed along Path B and was used to fluidize the agglomerated particles in the fluidizer. The pickup tube was connected to a tapping in the particle-shearing nozzle at a point where the nozzle flow reached Mach 2. At this point, the flow static pressure was below that of the fluidizer and hence, fluidized particles and agglomerates were forced into the shearing nozzle. The arrangement resulted in the transverse injection of particles and agglomerates into the Mach 2 stream. This had the effect of shearing the agglomerates and dispersing the resulting fine particles into the main flow. As the seeded flow was shocked down to subsonic velocity downstream of the nozzle, further particle shearing may have taken place. The method of particle shearing was based on the work of Ref. 6.

The seeding rate of the particle seeder was controllable though a remote valve which regulated the amount of flow running along Path B. Additionally, the outlet total pressure was controlled via a valve that allowed some flow to bypass both the fluidizer and the particle-shearing nozzle. This is illustrated as Path C in Fig. 2. Further details of the particle seeder design and operation are available in Ref. 1.

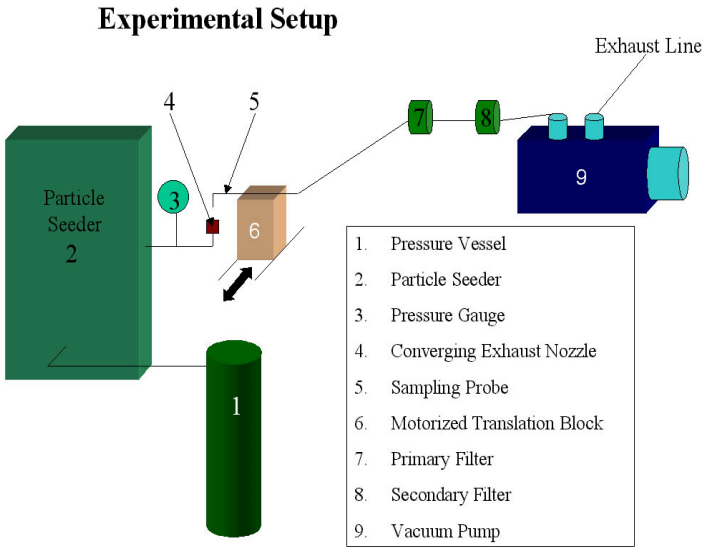

Fig. 1 Overview of experimental setup

Exhaust Nozzle

There were two primary design objectives for the exhaust nozzle. The first was the need to set the nozzle throat diameter close to that of the fuel injector used in the supersonic combustion tests of Refs. 1 and 2. Matching throat areas ensured that, at the same gas supply pressure, the stagnation pressure upstream of the exhaust nozzle approximately matched that of the fuel injector. This was important in order to ensure the experiment was accurately modeling particle shearing and dispersal behaviors as would actually occur during a supersonic combustion experiment. The second design objective was to minimize the possibility of flow recirculation within the nozzle. Recirculation could disrupt the normal particle distribution by causing some particles to adhere to the walls of the nozzle. This could lead to agglomerates forming downstream of the seeding apparatus. This condition was avoided by using a steadily converging nozzle. The nozzle was operated such that the pressure ratio across the nozzle during sampling was sufficiently high to drive the flow sonic at the throat.

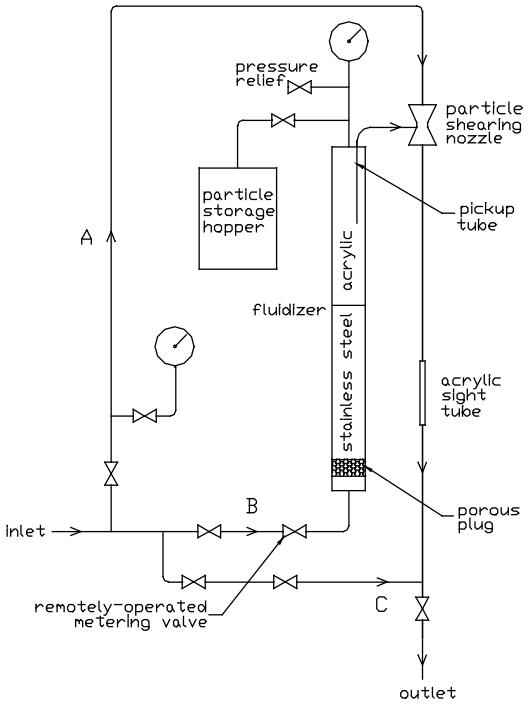

Fig. 2 Schematic of particle seeder (reproduced from Ref. 2 with permission)

Sampling Probe

The primary issue in the design of the sampling probe was choosing a sampling tube size that had a mass flow intake that would not exceed the maximum mass flow rate that could pass through the finest filter paper. This was

critical to ensure full capture of streamlines and, hence, that all particle sizes were sampled with equal probability. The probe sampling inner diameter was chosen assuming a Mach 1 (T=300 K) nitrogen jet and 0.2 μm Cellulose Nitrate Membrane filter paper. Under these conditions and at a nominal sampling point, the minimum filter paper mass flow rate would not be exceeded provided the sampling probe inner diameter was less than 1.66 mm. The actual probe was constructed of Inconel tubing with an inner diameter of 1.32 mm. After some preliminary experiments it was found that 0.1 μm filter paper was more effective at capturing particle samples and thus there was a need to sample at a point in the jet with a with a flow velocity less than that of the original calculation. This was a consequence of the lower maximum permissible volume flow rate of the finer (0.1μm) filter paper.

The sampling probe was also constructed with tapering outer walls at the probe inlet, such that the tube had an approximately 20-deg. sharp leading edge. This feature was incorporated to further decrease the chances of a bow shock induced spillage at the inlet to the probe.

Filtering Equipment

As mentioned above, in order to collect particle samples, the flow through the sampling probe was passed though a series of filter papers. The primary filter was the first in the series and had the finest mesh size. For the experiments, 47 mm diameter, 0.1μm Cellulose Nitrate Membrane paper was used. This was the finest paper that could be obtained. The paper was rated at a volumetric flow rate of 0.67 L/min./sq cm. The filter paper holder design was such that particles were captured over the full diameter of the paper. The particle samples that were imaged were collected using the primary filter paper. Interestingly, after analyzing SEM images, it was found that the filter paper had a surface mesh size substantially larger than the manufacturer's specified nominal size. The surface pore sizes for the 0.1 μm paper were found to be in the range of 0.04 to 0.25 μm. The secondary filter (0.2μm Cellulose Nitrate) was used solely as a backup to protect the vacuum pump from particle ingestion.

Experimental Methods

Test Rig Operating Variables

Nitrogen and helium were adopted as the gases into which the particles were seeded. During the supersonic combustion experiments of Refs. 1 and 2, particles were seeded into the hydrogen fuel. However, for the present study, using hydrogen was impractically hazardous. By using two gases of know composition, the results of the present study could be approximately extrapolated to hydrogen. For the experiments, the gas total pressure upstream of the seeding apparatus was maintained at 2 MPa. This resulted in a total pressure downstream of the seeder of 1 MPa and a pressure ratio across the exhaust nozzle of 9.9. The total temperature of the seeded gas was approximately 300 K throughout the experiments.

The seed particle adopted for the experiments consisted of Alumina (Al_2O_3). These particles had a manufacturer's specified nominal primary particle size of 0.3 μm and a density of 3940 kg/m^3. The nominal agglomerate size range during storage was approximately 4 to 40 μm. This type of particle was used in the PIV experiment of Ref. 1.

Probe Location

The axial placement of the probe inlet from the exit plane of the exhaust nozzle was determined by considering the maximum allowable flow rate through the probe at a no spillage condition. As noted above, it was critical that this flow rate be less than that allowed by the filter paper or else flow at the inlet of the probe would be stagnated. Measurements were performed at a distance of 64 mm downstream of the nozzle. In addition, the point of measurement was close to the jet centerline.

In order to determine the mass flux of the jet flow at the point of sampling, flow velocity was determined by using the sampling probe to measure the flow total pressure. Here the probe was connected to a pressure gauge, instead of the filter and vacuum pump assembly, and was used as a Pitot tube. In applying this technique, it was assumed that the static temperature and pressure of the jet had reached ambient conditions. The point of measurement was in the subsonic far field of the jet, well downstream of the under-expanded jet's Mach disk[7]. From a computed Mach number and the assumption the fluid was at room temperature, the flow velocity and thus mass flux could be determined.

Test Matrix

Trials were performed in two experiments. The details of each are listed in Table 1. The vacuum pump pressure listed in the table is the pressure measured downstream of the secondary filter while the probe was exposed to the jet. In addition, the exposure times refer to the elapsed time a particular piece of filter paper was exposed to the seeded jet flow. An exposure time of 30 sec. was found to result in the best concentration of particles on the filter paper for the imaging method outlined below. Therefore, the results of the 30 sec. tests are presented below.

In a separate experiment, a control test was conducted in order to establish the level of background particles present in the room air. This test was deemed necessary because

the vacuum pump was turned on prior to the probe being traversed into the seeded jet. The test was performed by running the vacuum pump with the jet flow turned off, such that the filter paper was exposed only to the air sampled from the laboratory. Using the imaging method outlined below, it was established that background room particle levels were not significant.

Table 1 Experiment test matrix

	Experiment 1	Experiment 2
Nozzle stag. pressure	1 MPa	1 MPa
Seeded gas	He	N_2
Particle type	0.3 μm Al_2O_3	0.3 μm Al_2O_3
Primary filter paper	0.1 μm	0.1 μm
Total press. at probe inlet	101 KPa	101 KPa
Probe location	63.8 mm	63.8 mm
Vacuum pump pressure (jet on)	80 KPa	80 KPa
Exposure time	15 sec	15 sec
	30 sec	30 sec
	1 min	1 min

Particle Sample Imaging

In order to image the sample particles, a Scanning Electron Microscope (SEM) was utilized. To mount the particles in the SEM, the filter paper was divided into halves and then mounted on an electrically conductive double-sided tape. Cutting the paper into halves ensured that half the sample would remain for future reference and also facilitated an easier fit of the samples onto the SEM mounting block. Once mounted, images could be generated at various magnifications at any location on the sample surface. Magnification levels were generally in the range of 200 to 50,000.

Image Processing Methodology

In order to obtain quantitative data from the SEM images, a manual technique was developed for counting particles and determining their sizes within an arbitrary reference area on the filter paper. The counting and measuring of particles was performed using an image viewing program. Using the software, it was possible to count the number of particles in a given image and also measure their characteristic size, or length, in pixels. Here the characteristic length was defined as a particle's longest linear dimension. This pixel measurement was then converted to a metric length using the reference scale of each image. This process could only be accomplished accurately if a series of images of varying magnification were used instead of a processing only a single image. This is because of resolution limitations of the SEM images and the fact that particle sizes varied by almost two orders of magnitude.

In this experiment, each data set was obtained by processing up to three different magnification images. The primary image was at a low enough magnification such that the largest particles on the filter paper could be easily counted and measured. After this image was processed, a second image of higher magnification was used to measure particles that were not easily resolvable in the first image. After these particles had been counted and measured the data was then extrapolated to the area of the larger primary image. For example, if the primary image were ten times the area of the second image, then particle counts in the second image were multiplied by 10 in order to scale them up to the area of the first image. Here it was assumed that particles of a given size were evenly distributed across the surface of the filter paper.

In some cases it was possible to choose images such that the largest particles from the higher magnification image would overlap in size with the smallest particles from the lower magnification image. Therefore, as a quality check of the counting and sizing method, the particles in the overlapping region of the high magnification image were extrapolated to the area of the low magnification image, and then the two results were compared. For example, in Experiment 1, two images had overlapping particles in the size range of 0.20-0.25 μm. For this particular experiment and size bin, the image of lowest magnification had a particle count within 7% of the value obtained by area scaling data from the highest magnification image. This calculation was based on a particle count of 16 for the specified bin size in the low magnification image. Comparisons such as these, confirmed the existence of a relatively small error in the counting and sizing method. When tabulating the final results, careful care was taken such that the same particles were not counted twice. Consequently, only the data from one image was used in the case of overlapping particle sizes.

As mentioned above, up to three different image magnifications were used to generate each data set. Thus, the process described above was repeated a third time for some cases, on the image of highest magnification. For the cases presented in this work, the highest magnification image was either 6×4 μm or 4×4 μm in size. As described above, the results obtained at this magnification were extrapolated to the area of the primary low magnification image. Because the area difference between this high magnification image and that of the lowest magnification image was typically quite high, the results obtained at the highest magnification were very important since they represented a large proportion of the

total particle count. Therefore, particular care was taken in counting particles at this magnification.

Figure 3 illustrates the general image processing methodology. The large figure on the left is the primary low magnification image. The image in the upper right of the figure is of medium magnification and the third image is of high magnification. The arrows illustrate how the higher magnification images are a smaller interrogation region of the larger image. Although Fig. 3 suggests that the smaller interrogation regions were actually in the same field of view as the higher magnification image, this was is not necessarily the case. It is assumed that each interrogation region is representative of the sample as a whole and thus it is not necessary for all analyzed images to be in the same field of view.

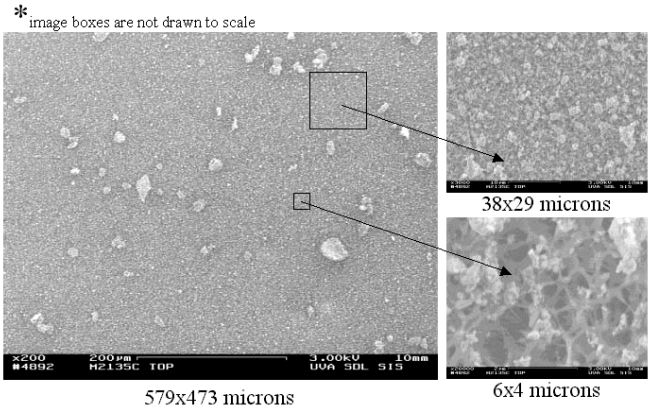

Fig. 3 Image processing methodology (tests using 0.2 μm Cellulose Nitrate as primary filter)

It is noted here that an effort was initiated to automate the counting and sizing process described above. This was attempted through the use of the image processing toolbox in MATLAB®. Two codes were written in this attempt. The first could identify and measure mean diameters of particles in an image provided they were in stark contrast to a homogenous background and that the particles were not touching one another. The second code developed made use of a process called Watershed Segmentation in order to detect individual particles and measure their respective sizes even when they were touching and overlapping other particles. Watershed Segmentation is described in the MATLAB® help files. Each of these codes exhibited encouraging success when tested on artificial, ideal images. However, when the codes were tested on the more complicated images acquired in this study, the results were unreliable. This difficulty was due in part to the fact that the filter paper membrane background was not homogenous. As can be seen in Fig. 3 and in Fig. 4, at high magnifications, the filter membrane appeared as an inconsistent, complex web and pore structure. This background made it difficult for the developed codes to identify individual particles.

RESULTS & DISCUSSION

Particle Shape

One of the objectives of this study was to determine the shapes of the sampled seed particles. As can be seen in Figs. 3-5 particles were rounded, irregular or ligamental in nature[8]. In general, particles smaller than 0.1 μm, (see Fig. 4), were irregular in shape. While, particle shapes in the 0.1 to 1 μm range were found to be a mixture of rounded, irregular and ligamental. As is also evident in the figures, particles larger than 1 μm, or agglomerates, tended to be more rounded than their individual constituents. In general, agglomerates were the closest to approximating a theoretical spherical shape.

No general trend was observed between the shapes of the particles and the seeded gas type. However, one noticeable result was that the particles seeded into helium were generally smaller, with fewer agglomerates. This topic is the subject of the discussion below.

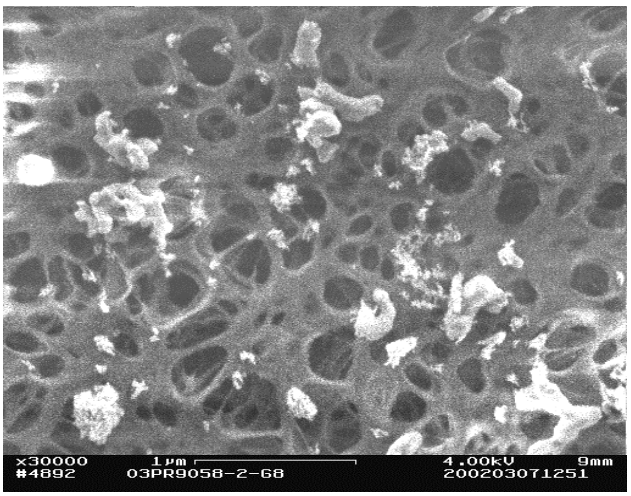

Fig. 4(a) Particle shapes (Exp. 1)

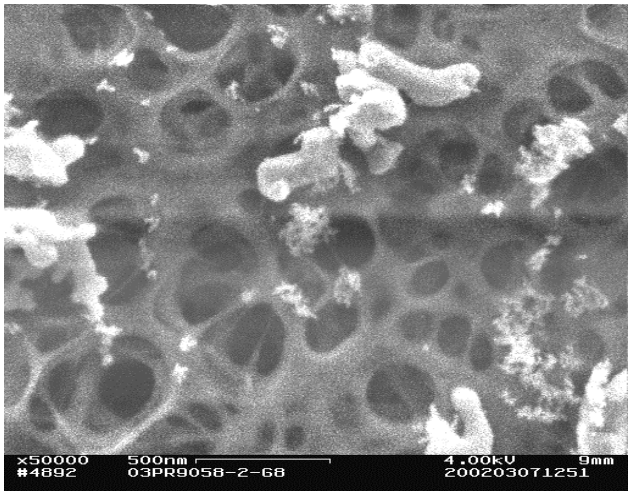

Fig. 4(b) Particle Shapes (Exp. 1)

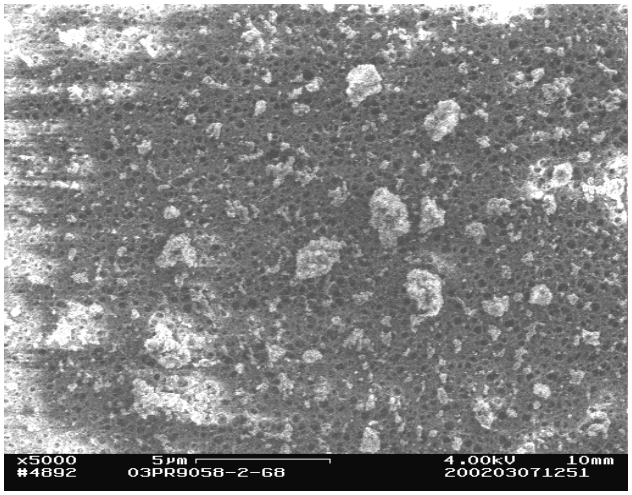

Fig. 5 View of large agglomerates (Exp. 1)

Particle Size

Reported in this section are the size distribution results obtained for the two experiments as defined in Table 1. For each case, a histogram of particle size was determined and used to calculate the cumulative size distribution. Size histograms and cumulative distributions are presented for Experiments 1 and 2 in Figs. 6 and 7, respectively. The histograms presented have been truncated at 1 µm in order to show detail at small particle sizes. For each experiment, the larger particles size bins that were truncated collectively accounted for less than a few percent of the total particle count. For Experiments 1 and 2, particles as large as 2.89 µm and 2.46 µm, respectively, were counted. The data displayed for Experiment 1 is based on the measurement of 122 particles and the processing of 3 separate images. While for Experiment 2, the displayed data is based on the measurement of 63 particles and two separate images.

Comparing Figs. 6 and 7, it is evident that, when compared to the data of Experiment 2, the size distributions for Experiment 1 are shifted towards smaller sizes. There are also fewer particles in the "tail" of the distribution for Experiment 1. These findings are a consequence of the fact that the seeded gas was helium for Experiment 1 and was nitrogen for Experiment 2. In the shearing nozzle of the seeding apparatus, the speed of sound in helium is approximately three times higher than that for nitrogen. Thus, the magnitudes of the velocities in the shearing nozzle are also approximately three times higher for helium. Therefore, the shear forces on the particle agglomerates, induced by the transverse injection of particles into the shearing nozzle, are expected to be higher for helium. This results in smaller final particle sizes for helium than for nitrogen, as is evident in Figs. 6 and 7. The mean characteristic particle length for each experiment was also in line with this argument. For Experiment 1 with helium, the mean length was 0.23 µm. While, for Experiment 2, with nitrogen as the seeded gas, the mean particle size was 0.49 µm.

Light Scattering Distribution

As outlined above, the light scattering and flow tracking characteristics of seeded particles is of critical importance for particle based flow diagnostic techniques. Therefore, using determined particles size distributions, these two aspects are now considered in turn. Because helium has the closest thermodynamic properties to the hydrogen fuel used for the experiments of Refs. 1 and 2, the results of Experiment 1 are considered here.

Using the particle size distribution of Fig. 6(a), a light scattering cross section distribution was calculated. Light scattering cross section, $C_{s,}$ is defined as per Ref. 3 below.

$$C_s \equiv \frac{P_s}{I_o}$$

Here P_s is the total scattered power and I_o is the laser intensity incident on the particle. Results based on the particle size distribution of Exp. 1 are plotted in Fig. 8. The plot was generated based on the assumption that the particles scatter light according to Mie theory[3,5], which is a valid assumption for the particle sizes considered in this study. Mie scattering theory applies to spherical particles, thus the results are only approximate. For all particle sizes considered in this study, C_s was assumed to scale with the particle characteristic length raised to the sixth power. It is noted here that observed light intensity is not solely a function of C_s, but also a function of the observation angle, which is also sensitive to particle size[3].

However, for the present demonstration this effect is neglected.

It can be seen in Fig. 8 that a large proportion of the scattering cross section is due to the largest particles. In fact, just over 50% of the distribution can be attributed to particles in the 0.9-1.0 μm size range. Referring to Fig. 6(a), particles in this size range account for just 2% of the particle size distribution. This result highlights the need to adjust PIV and FPI particle imaging equipment such that sufficient signal to noise ratio is obtained for the particle size range of interest, and not for particles scattering the greatest intensity.

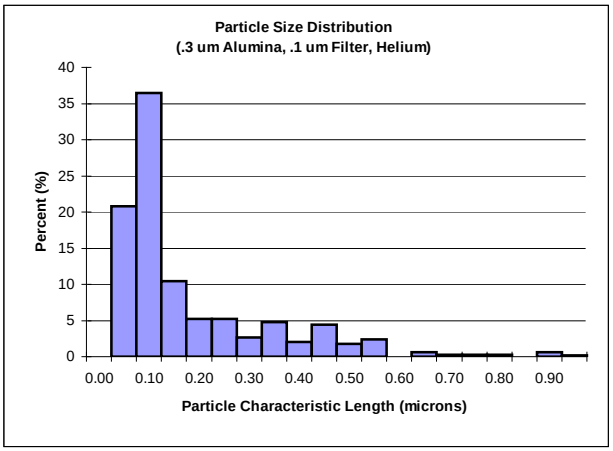

Fig. 6(a) Experiment 1 particle size histogram

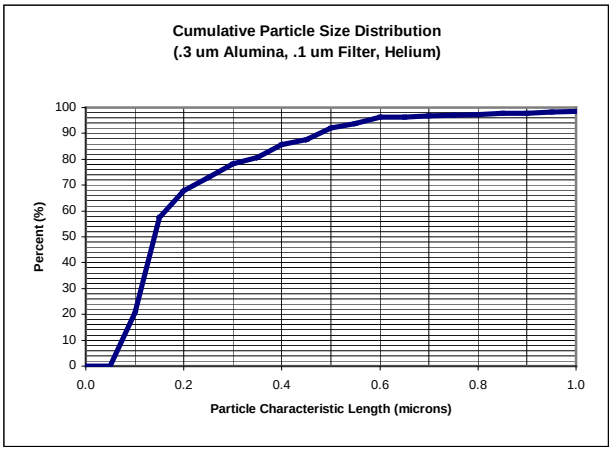

Fig. 6(b) Experiment 1 cumulative particle size distribution

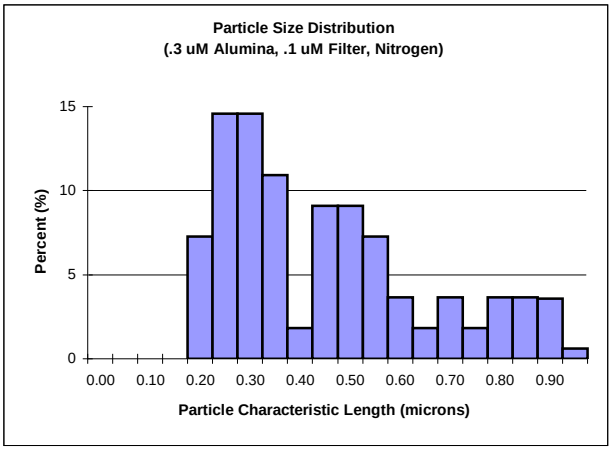

Fig. 7(a) Experiment 2 particle size histogram

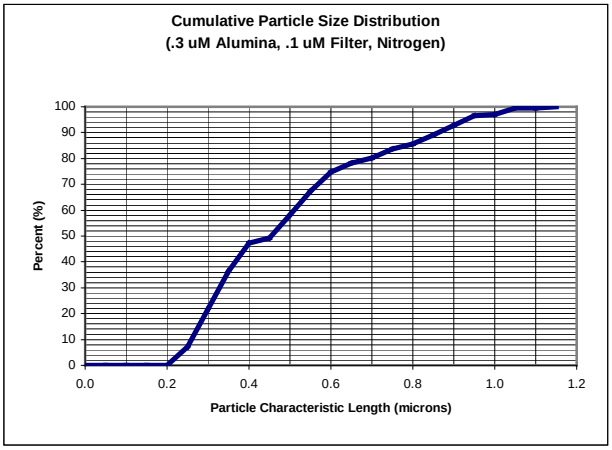

Fig. 7(b) Experiment 2 cumulative particle size distribution

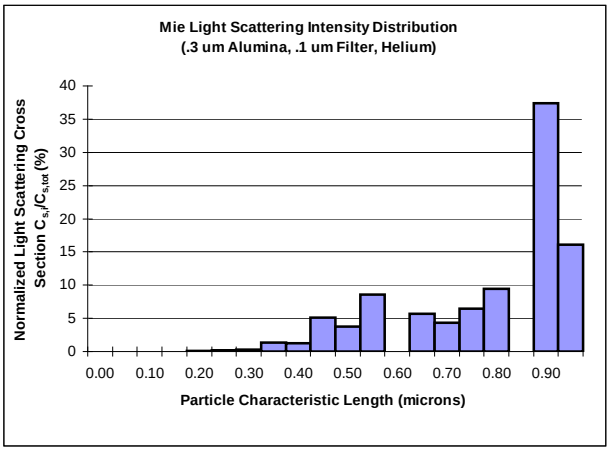

Fig. 8 Normalized Mie light scattering cross section for Experiment 1

Flow Tracking Distribution

As an example of how particle size distribution data can be used to quantify the flow tracking errors present in a particle based diagnostic, the simple case of flow through an oblique shock is considered. This oblique shock case is a strong test of particle flow tracking ability since the step change in fluid velocity across the shock is virtually instantaneous. The particle's ability to track this change in velocity is a measure of its flow tracking ability. The case considered is a shock generated by a 10-deg wedge in a Mach 2 flow with a flow velocity of 1030 m/s. This geometry and flow condition results in a shock strength that is representative of conditions encountered in the supersonic combustor tests of Refs. 1 and 2. The test case is schematically depicted in Fig. 9. The velocity vectors shown correspond to the streamline velocities before and after the shock, v_1 and v_2, respectively, and the velocities normal to the shock wave, v_{1n} and v_{2n}, respectively. In the flow tracking calculations presented here, particles of various diameters subjected to the flowfield immediately behind the oblique shock wave were considered. In addition, the change in velocity normal to the shock was used in the calculations since this is the component that changes across the shock. As explained by Refs. 3 and 4, the response of a particle to a step change in gas velocity is exponential and can be approximated using Stokes drag. The further downstream a particle takes to decelerate to the new gas velocity, the poorer its flow tracking capability. Larger particles will take longer to respond to the shock because of their increased inertia and thus will exhibit poorer flow tracking than smaller particles.

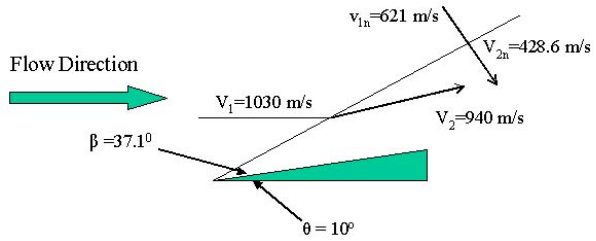

Fig. 9 Oblique shock formation in air on a 10-deg wedge

Particle trajectories behind the oblique shock were simulated for various particle diameters using a Stokes drag coefficient with a compressibility correction[4]. It is important to note that the model is based on a spherical particle. As discussed above, this is an approximation for the particles sampled in this study, particularly for particle sizes below 1 μm. The input parameters for the calculations are summarized in Table 2.

Table 2 Flow tracking calculation input parameters

Parameter	Value
V_{n1} (m/s)	621.0
V_{n2} (m/s)	428.6
Particle density (kg/m^3)	3940
Gas density behind shock (kg/m^3)	0.37
Specific heat ratio behind shock	1.34
Gas constant behind shock (J/kgK)	287
Static temp. behind shock (K)	746.3

The particle drag model was combined with the particle distribution data of Fig. 6(a) to determine the proportion of particles that are able to effectively track the flow as the particles proceed downstream from the shock. The distribution data that was adopted was obtained for seeded helium of Experiment 1. The results are presented in Fig. 10 as a plot of the proportion of particles tracking the flow velocity, to within a certain percentage, as a function of the normal distance downstream of the shock. This percentage was chosen to be 10% and defines the point as which the particles may be considered to be effectively at the new gas velocity.

Figure 10 yields some important findings and implications for particle based diagnostics using the tested particles. First, for the given particle size distribution, there is zero probability that particles will be tracking the flow accurately over the first 0.6 mm normal to the shock. Consequently, if a PIV experiment, for example, were being performed on this flowfield, it would be unwise to consider data points taken in the first 0.6 mm to be an accurate representation of the flow behavior. Referring again to Fig. 10, an estimate can be made as to the point where the majority of the particles will be tracking the flow. It can be seen that 90% of the particles will be tracking the flow effectively at a distance of 3.6 mm normal to the shock wave. Therefore, in a PIV measured velocity field, for example, the shock wave will appear smeared over a distance of 3.6 mm and the experimental error over this distance will be high. However, as noted by Ref. 1, such flow features can only be spatially resolved to within the resolution of the particle based diagnostic in any case. For the high speed measurements of Ref. 1, this resolution was of the order of 1 mm. Hence, an acceptable spatial extent of velocity lag is somewhat dependent on the nature of the diagnostic.

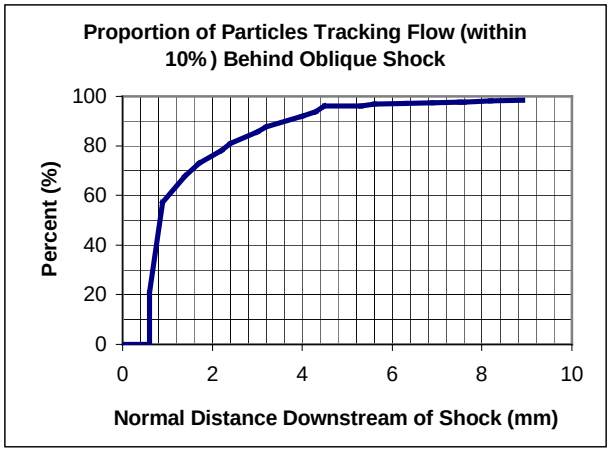

Fig. 10 Effect of Exp. 1 particle size distribution on particle tracking behavior downstream of an oblique shock wave

The preceding discussion is a simple example of how particle distribution data can be used to either plan a particle diagnostic experiment more effectively or interpret results more accurately. This type of analysis could also be extended to a more complicated computational simulation provided the ability of the particle to track the flow is still directly related to its size (as was the case in the example above). Assuming this assumption holds true, a three-dimensional computational model could be used to model the interaction of seed particles with, for example, ramp induced vortices involved in the fuel-air mixing process of the supersonic combustor of Ref. 2. Such an analysis could thus be used to examine particle lag errors in the FPI measurements of Ref 2.

CONCLUSIONS

This paper has presented a method for assessing the performance of a particle seeding apparatus. The developed method was applied to a seeder that was previously used for PIV and FPI measurements in order to obtain qualitative particle shape information and quantitative particle size distribution data. One outcome of the analysis of this data was that the Alumina particles sampled in this study were not spherical, although the agglomerates larger than 1 μm were closer to being spherical then the primary particles themselves. Primary particles were found to be rounded, irregular or ligamental in nature. The second major outcome of this study is the quantitative particle distribution data presented in Figs. 6 and 7. These results show that when nitrogen was the seeded gas, particles had a mean characteristic length of 0.49 μm. When helium was used as the seeded gas, the average particle size was 0.23 μm, approximately half that for nitrogen. In addition, using a combination of the particle distribution data and Mie scattering theory, it was shown that a very small proportion of large particles can still effectively dominate a scattered light signal. Lastly, using the particle distribution data for helium, it was shown how such data can be used to assess particle lag errors of an optical diagnostic technique such as FPI or PIV.

Several important conclusions can be drawn based on the experimental data collected in this experiment. First, since the Alumina particles considered in this study were found to be a mix of non-spherical shapes, care should be exercised when using a particle sizing technique that assumes a spherical particle.

Second, based on the particle size data it was demonstrated that the seeding apparatus was very effective at breaking down naturally occurring agglomerates. Agglomerates were expected to be in the size range of 4 to 40 μm and it was demonstrated that almost 100% of the generated seed particles were sub-micron in size, regardless of the type of gas seeded.

Third, the evidence strongly suggests that particles are smaller when the acoustic velocity of the seeded gas is higher. This is a consequence of the operation of the particle-shearing nozzle of the seeder. The shearing nozzle imparts greater shear forces on particle agglomerates when the speed of sound of the seeded gas is higher. Based on this finding, it is expected that hydrogen would result in smaller particles than helium since its acoustic velocity is higher. With additional data points, obtained using other gases, a scaling law could be deduced that allows reliable extrapolation of particle distributions to gases such as hydrogen. However, if a simple linear relation is adopted as an example, and the speed of sound of hydrogen is compared with that of nitrogen and helium, the present data would suggest that particles with a mean size of less than 0.2 μm and approaching 0.1 μm could be obtained with hydrogen. Further investigation of particle size scaling is proposed as a valuable topic for future study.

And lastly, a more objective method of counting and sizing particles needs to be developed. The manual operation described in this study is time consuming and prone to inaccuracies and biases. With the abundance of high performance image processing software available on the market, an accurate automated method may yet be found.

Although the particle sampling, sizing and counting methods developed in this study were designed to minimize systematic biases, it may be argued that significant biases still exist. Not withstanding the manual sizing and counting technique adopted, the collection and sampling via filter paper may be biased towards relatively

large particles. The 0.1 μm filter paper was found to have surface pores with diameters in the range of 0.04 to 0.25 μm. Thus, particles smaller than 0.25 μm are less likely to be sampled and counted. However, the results obtained are encouraging in terms of flow tracking errors present in past and future particle based diagnostics that are conducted using the tested particles and seeding apparatus. Mean seeded particle sizes were measured to be at best 25% below the nominal 0.3 μm size for the particle type tested. Thus, when the above systematic biases and the thermodynamic properties of the seeded gas are considered, even better results may be expected when the particles are seeded into the hydrogen fuel of scramjet combustor tests. Superior seeder performance may be also be obtained if alternate particle types are tested.

ACKNOWLEDGEMENTS

This research was funded by NASA through grants NAG-1-2131 and NAG-1-02019 with C.R. McClinton and D.E. Reubush of the NASA Langley Research Center as technical monitors.

REFERENCES

[1]Goyne, C.P., McDaniel, J.C., Krauss, R.H., and Day, S.W. "Velocity Measurement in a Dual-mode Supersonic Combustor using Particle Image Velocimetry." AIAA Paper 2001-1761, April 2001.

[2]Goyne, C.P., McDaniel, J.C., Quagliaroli, T.M., Krauss, R.H., and S.W. Day. "Dual-Mode Combustion of Hydrogen in a Mach 5, Continuous-Flow Facility." *Journal of Propulsion and Power* Vol. 17, No. 5, 2001.

[3]Melling, A. "Tracer Particles and Seeding for Particle Image Velocimetry." *Meas. Sci. Technol.* 8 (1997): 1406-1416.

[4]Meyers, J.F. "Generation of Particles and Seeding." von Karman Institute for Fluid Dynamics. Lecture Series 1991-08, June 1991.

[5]Ledig, S.H., Donohue, J.M., and J.C. McDaniel. "MIE Scattering for Mixing Measurements in Nonreacting Supersonic Flowfields. " 31st AIAA/ASME/SAE/ASEE Joint Propulsion Conference and Exhibit. San Diego, CA, July 10-12, 1995.

[6]Smith, M.W., "Application of a Planar Doppler Velocimetry System to a High Reynolds Number Compressible Jet," AIAA Paper 98-0428, Jan. 1998.

[7]Ashkenas, H., and Sherman, F.S., "The Structure and Utilization of Supersonic Free Jets in Low Density Wind Tunnels," in de Leeuw, J.H., ed., Rarefied Gas Dynamics, Proceedings of the Fourth International Symposium on Rarefied Gas Dynamics, Supplement 3, Volume II, Academic Press, New York, 1966.

[8]German, R.M., *Powder Metallurgy Science*, Metal Powder Industries Federation, Princeton, 1984.